HEALTHY HUMAN B-CELL AGING CHARACTERIZED BY REGULATORY-STATE REMODELING *

Yifan Wang[1,*], **Lanxin Ma**[1], **Jingwen Zhang**[1]
[1]CIS, Westlake University, Hangzhou, China
*Correspondence: corresponding.author@email.edu

ABSTRACT

Aging is accompanied by impaired antibody and vaccine responses, yet it remains unclear whether human B-cell aging is driven primarily by loss of major cellular compartments or by subtler changes in cell state. We analyzed the processed OneK1K single-cell object, which retained 1,248,980 peripheral blood mononuclear cells from 981 of the 982 originally reported donors aged 19–97 years, including 129,579 re-annotated B cells. To preserve the donor as the biological replicate, we separated compositional analyses from donor-by-subtype pseudobulk expression analyses and modeled age continuously, with spline-based assessment of nonlinearity. Uncorrected binomial models suggested a decline in memory B cells and an increase in intermediate B cells; however, marked donor-level overdispersion, a largely stable combined memory–intermediate compartment, and the absence of an age-related shift along a discovery-defined continuous memory–intermediate axis indicated substantial sensitivity to discrete label boundaries. In contrast, subtype-intrinsic transcriptional remodeling was coordinated across genes, pathways, and inferred regulons. Memory B cells showed increasing expression of *CD69*, *NR4A2*, *BTG1*, and *LGALS1*, together with inflammatory and stress-associated pathway enrichment and reduced MYC/E2F-associated proliferative readiness. Naive B cells showed stronger interferon-associated programs. Across naive, memory, and intermediate B cells, FOXO3-associated regulon scores increased from age 40 to 80 years (estimated changes 0.143, 0.173, and 0.188 ULM units; false-discovery rates 0.0048, 0.0082, and 0.00489), whereas a PAX5-associated identity-maintenance program decreased specifically in intermediate B cells (-0.250 ULM units; false-discovery rate 1.12×10^{-5}). STAT1- and NF-κB-associated programs showed convergent support but did not meet the same global false-discovery threshold. All six prespecified core regulatory effects were directionally concordant in an age- and sex-stratified split-half analysis. These results support a model in which healthy human B-cell aging is characterized less by major compartment depletion than by small, coordinated, and subtype-resolved shifts toward inflammatory vigilance, stress adaptation, altered identity maintenance, and reduced readiness for clonal expansion.

Keywords B-cell aging · immunosenescence · single-cell RNA sequencing · pseudobulk · FOXO3 · PAX5 · regulon · OneK1K

1 Introduction

Aging reshapes the immune system and is associated with weaker responses to infection and vaccination, increased low-grade inflammation, and greater susceptibility to autoimmunity and hematologic disease. B cells are central to humoral immunity through antigen recognition, antibody production, antigen presentation, and the formation of immunological memory. Age-related defects in B-cell activation, class-switch recombination, germinal-center participation, and clonal expansion are therefore plausible contributors to the reduced quality and durability of antibody responses in older adults [Goodwin et al., 2006, Frasca et al., 2008]. Population-scale and single-cell studies further indicate that immune aging is nonlinear and cell-state dependent [Mogilenko et al., 2022, Terekhova et al., 2023].

*This work is developed during the 2026 PEBBLE BioFusion Workshop at Westlake University in Hangzhou, China, from July 24th to August 4th.

Previous work has identified age-associated B-cell populations with atypical or chronically stimulated phenotypes. In mice, CD11c-positive age-associated B cells accumulate with age and can respond strongly to innate immune signals [Hao et al., 2011, Rubtsov et al., 2011]. In humans, phenotypically related CD21-low, CD11c-positive, and T-bet-positive populations have been linked to aging, chronic infection, and autoimmunity. Particularly relevant to the present study, Nipper et al. [2018] reported that diminished antibody responses to influenza vaccination in older adults were associated with expansion of an age-associated B-cell population with low PAX5 expression. PAX5 is a core regulator of B-lineage identity and function, making this observation a potential bridge between altered B-cell composition and altered lineage-maintenance programs [Nutt et al., 1999, Cobaleda et al., 2007].

The OneK1K resource established a population-scale foundation for resolving immune regulation at single-cell resolution. Yazar et al. [2022] profiled 1,267,758 peripheral blood mononuclear cells from 982 donors and mapped 26,597 independent cis-expression quantitative trait loci across 14 immune cell types. Importantly for B-cell biology, they showed that genetic effects were not fixed across discrete labels: among 1,988 eSNP–eGene pairs expressed across the B-cell maturation landscape, 333 showed significant changes in allelic effect as cells transitioned from naive to memory states. This observation established the naive-to-memory continuum as a biologically meaningful context in which regulatory effects can vary, but the study was designed primarily around genetic regulation and autoimmune-disease loci rather than aging.

A subsequent analysis by Sopena-Rios et al. [2026] used the same OneK1K resource to study age and biological sex across 982 adults. Their immune-wide analysis identified sexually dimorphic compositional and transcriptional trajectories, with more extensive remodeling in female participants and an age-associated expansion of a B-cell population linked to an asymptomatic precursor state of chronic lymphocytic leukemia in a subset of male participants. This study is the closest published comparator to the present work. Because both analyses derive from OneK1K, it should not be treated as independent replication. Rather, it defines the immediate analytical context for a complementary B-cell-focused investigation of major subtype architecture, donor-level transcriptional remodeling, and inferred regulatory programs.

Several analytical questions remain open even in large single-cell cohorts. Young-versus-old contrasts can obscure gradual or nonlinear trajectories; abundance and within-subtype expression can be conflated; and treating individual cells as independent biological replicates can produce pseudoreplication and anti-conservative P values [Squair et al., 2021, Crowell et al., 2020]. Discrete clustering can also convert modest redistribution near a state boundary into apparently large changes in subtype abundance. Finally, transcription-factor analyses restricted to a small candidate list can underestimate the multiple-testing burden. These issues motivated an analysis that separated composition from cell-intrinsic expression, used the donor as the statistical replicate, modeled age continuously, and evaluated regulons across the full transcription-factor testing space.

Here, we used the OneK1K population-scale single-cell dataset to define how B-cell composition, subtype-intrinsic transcriptional programs, biological pathways, and transcription-factor-associated regulons vary across the adult lifespan. We asked four linked questions: whether the proportions of major B-cell subtypes change with age; whether apparent compositional changes are robust to overdispersion and cluster-boundary sensitivity; whether gene and pathway changes occur within stable compartments; and which shared or subtype-specific regulatory programs best summarize those changes. Our analysis was designed around the principle that the donor, rather than the individual cell, is the biological replicate. We hypothesized that healthy B-cell aging would be better explained by coordinated state remodeling than by wholesale loss of major B-cell compartments.

2 Methods

2.1 Study cohort and single-cell dataset

We analyzed the OneK1K peripheral blood mononuclear cell dataset generated by Yazar et al. [2022]. The original OneK1K publication reported 1,267,758 cells from 982 healthy donors. The processed working object supplied for the present analysis contained 1,248,980 cells from 981 donors aged 19–97 years (mean age, 63.9 years). The exact reason for the one-donor difference must be documented from the final preprocessing log before submission. Biological sex was recorded for 565 female and 416 male donors. The cohort was predominantly of European ancestry. All analyses were secondary analyses of the existing dataset.

2.2 B-cell re-annotation and donor coverage

B cells were re-annotated into four major groups: naive B cells, memory B cells, intermediate B cells, and plasmablasts. The resulting B-cell compartment comprised 129,579 cells: 65,702 naive B cells, 30,234 memory B cells, 29,889

intermediate B cells, and 3,754 plasmablasts. Donor-level analyses required a minimum number of 20 cells per donor. Plasmablast analyses were treated as exploratory because relatively few donors met higher cell-count thresholds.

2.3 Compositional analysis

For each donor, subtype counts were divided by the total number of B cells to obtain donor-level subtype fractions. Age associations were summarized per 10-year increase. Standard binomial generalized linear models were compared with quasi-binomial models to account for extra-binomial donor-to-donor variation, and Pearson overdispersion parameters were inspected directly. Because memory and intermediate B cells formed an adjacent and partially continuous transcriptional region, we performed a label-sensitivity analysis in which these two groups were combined. We also constructed a continuous memory–intermediate state score using weights learned in the discovery half and tested its association with age in the replication half.

2.4 Donor-by-subtype pseudobulk expression analysis

Raw UMI counts were summed by gene within each donor and B-cell subtype, yielding a donor $\times$ subtype $\times$ gene pseudobulk matrix. This design prevented hundreds of cells from one donor from being treated as hundreds of independent people. Composition and expression were analyzed separately so that an increase in the abundance of a subtype could not be misinterpreted as increased expression within that subtype. Age was modeled primarily as a continuous variable, with linear effects reported per 10 years. Flexible spline models were used to evaluate nonlinear trajectories. Young-versus-old contrasts and extreme-age comparisons were treated as sensitivity analyses rather than the primary inferential framework.

2.5 Pathway enrichment analysis

Genes were ranked by their age-association statistics within each subtype and analyzed by gene set enrichment analysis using the MSigDB Hallmark collection [Subramanian et al., 2005, Liberzon et al., 2015]. Pathways were interpreted only when the direction was coherent with leading-edge gene effects and was not strongly associated with technical covariates. Strongly negative ribosomal and translation-related enrichment scores were flagged as technically uncertain because they tracked library size, cell number, and ribosomal fraction; these signals were not interpreted as evidence of reduced protein-synthesis capacity.

2.6 Transcription-factor-associated regulon analysis

Transcription-factor-associated activities were inferred from donor-level pseudobulk expression with decoupler [Badia-i Mompel et al., 2022]. We used two prior-knowledge resources, CollecTRI and DoRothEA, and two complementary methods, univariate linear modeling (ULM) and multivariate linear modeling (MLM) [Garcia-Alonso et al., 2019, Muller-Dott et al., 2023]. Tests were corrected across the full space of 1,163 transcription factors and the analyzed B-cell subtypes, rather than only across a prespecified candidate list. We classified results as *strict* when they passed the global false-discovery threshold and as *convergent* when they showed agreement across networks, methods, and matching Hallmark pathways but did not pass the same global threshold. Inferred regulon activity was described as an associated target-gene program; it was not interpreted as a direct measurement of transcription-factor protein abundance, phosphorylation, nuclear localization, or causal activation.

2.7 Internal replication and sex-interaction analysis

The 981 donors were stratified by age tertile and sex and divided into a discovery set ($n = 490$) and a replication set ($n = 491$). Core regulatory findings were selected in the discovery set and then evaluated for direction, effect magnitude, and confidence intervals in the replication set. Age-by-sex interactions were tested for the six core regulatory effects only. Because these analyses were performed within a single cohort, they were considered internal replication rather than external validation.

2.8 Young-versus-old and variance sensitivity analyses

As a secondary analysis, donors aged 20–30 years were classified as young ($n = 47$ in the all-B analysis) and donors aged 80–90 years as old ($n = 142$). Donor-level full-transcriptome pseudobulk counts were analyzed with PyDESeq2 version 0.4.12. The primary dichotomous model used group alone, whereas a batch-robust sensitivity analysis used pool and group and was restricted to 20 pools containing both young and old donors. Genes were retained when they had at least 10 counts in at least 10 samples; differential expression required adjusted $P < 0.05$ and absolute $\log_2$ fold change

> 0.5. Hallmark preranked GSEA used Wald statistics and 1,000 permutations. For decade-level variance analyses, expression was normalized as $\log_2(\mathrm{CPM} + 1)$. Variance and coefficient of variation were summarized by decade for the reported differential-gene set and for 9,401 globally expressed genes. Robustness analyses used pool-residualized expression and a restriction to donors with at least 50 B cells.

2.9 Statistical reporting

Effect estimates are reported with confidence intervals where available. False-discovery rates were controlled by the Benjamini–Hochberg procedure within the prespecified testing spaces. Nominal P values from exploratory interaction or sensitivity analyses are labeled explicitly.

3 Results

3.1 Population-scale coverage of B-cell aging

The cohort covered nearly eight decades of adult life and included 129,579 B cells from 981 donors. Naive, memory, and intermediate B cells were represented across hundreds of donors, whereas plasmablast coverage was substantially lower. This scale enabled donor-level estimates of small average age effects while retaining the between-person variability expected in healthy populations (Fig. 1). The donor-level workflow explicitly separated composition from donor-by-subtype pseudobulk expression (Fig. 2). B-cell number per donor and pseudobulk library size were only weakly correlated with age in the secondary analysis ($r = -0.058$ and $r = -0.02$, respectively), arguing against a simple sequencing-depth explanation for age-associated expression patterns (Supplementary Fig. 14).

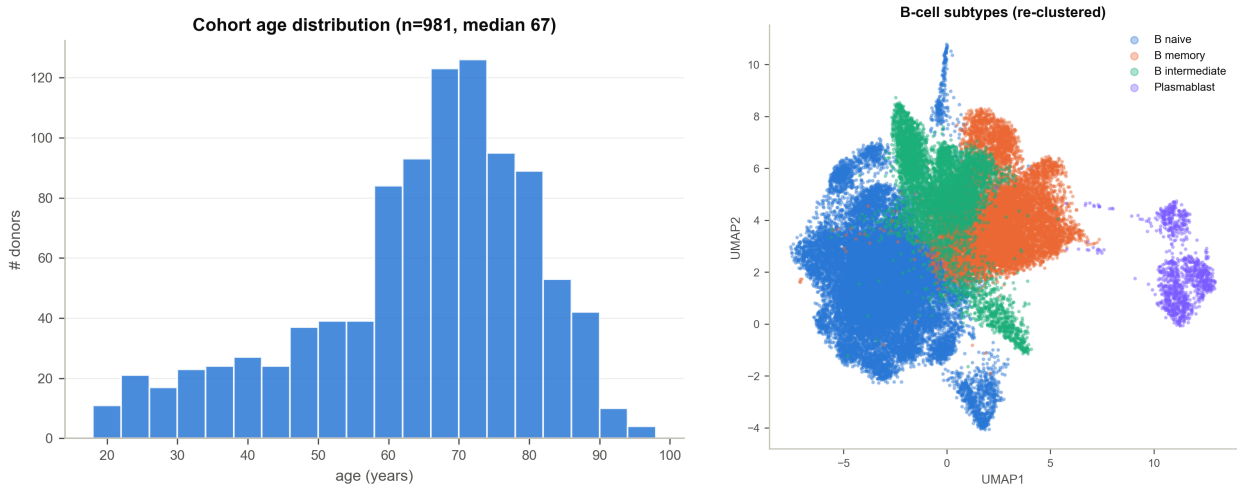

(A) Age distribution of the 981 analyzed donors.

(B) UMAP of the re-annotated B-cell populations.

Figure 1: A population-scale view of B-cell aging. The processed OneK1K object included 981 donors spanning 19–97 years and 129,579 re-annotated B cells. The UMAP resolves naive, memory, intermediate B cells, and plasmablasts. Donor coverage at alternative cell-count thresholds is shown separately in Supplementary Fig. 9.

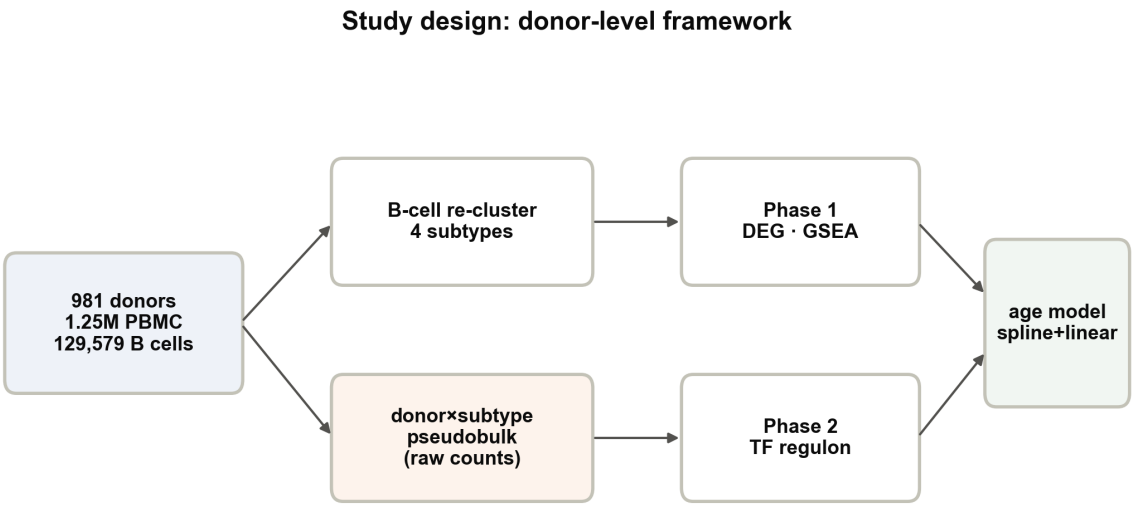

Figure 2: Donor-level analytical framework. B cells were re-clustered into four major subtypes. Composition was analyzed at the donor level, while raw UMI counts were summed within donor–subtype combinations for pseudobulk gene, pathway, and regulon analyses. Continuous and nonlinear age models were followed by split-half replication. The donor, rather than the individual cell, was the biological replicate.

3.2 Apparent memory loss is sensitive to overdispersion and label boundaries

At the level of discrete subtype labels, memory B cells appeared to decline by approximately 6.2 percentage points across the observed age range, whereas intermediate B cells increased by approximately 4.7 percentage points; naive B cells showed a smaller apparent increase (Fig. 4). Standard binomial models produced very small P values for several subtypes. However, Pearson overdispersion parameters ranged from 8.7 to 22, indicating substantially greater donor-to-donor variation than assumed by a binomial model. Quasi-binomial correction widened confidence intervals and removed the apparent significance of the naive B-cell change (Fig. 3A). A separate extreme-age analysis provided a second warning: 45 apparent intermediate-B-cell DEGs in the unadjusted contrast fell to zero after within-pool correction (Fig. 3B).

The opposing changes in memory and intermediate labels largely canceled when the two populations were combined: the memory–intermediate compartment declined by only 1.6 percentage points and was not significant. Moreover, a continuous memory–intermediate score, defined in the discovery half and tested in the replication half, showed no detectable age shift (coefficient approximately zero; $P = 0.97$ and 0.52 in the two split-half evaluations). Thus, the data did not support a global movement of cells along the continuous memory–intermediate axis. Instead, the most defensible interpretation is that modest changes in density near an artificial clustering boundary can create an apparent memory decrease and intermediate increase without substantial contraction of the broader memory-related compartment.

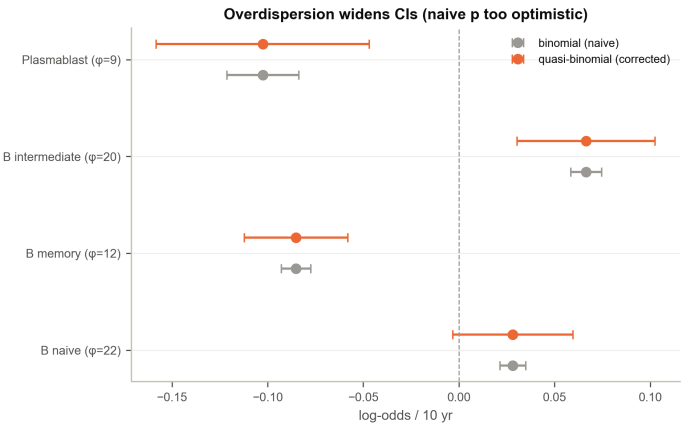

(A) Binomial and quasi-binomial age-effect estimates.

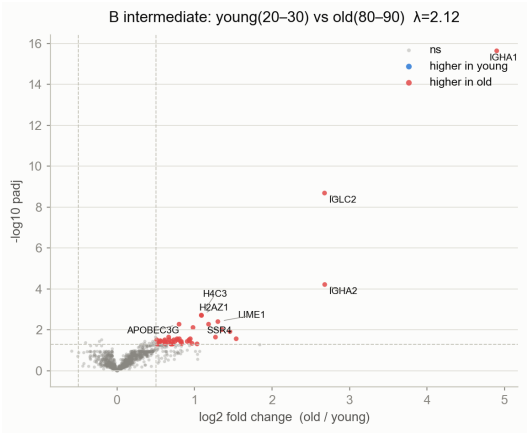

(B) Unadjusted young–old contrast in intermediate B cells.

Figure 3: Naive analyses can mistake donor heterogeneity, technical structure, or label effects for aging biology. **(A)** Donor-level overdispersion substantially widened confidence intervals relative to an ordinary binomial model. **(B)** The unadjusted 20–30 versus 80–90 year comparison yielded 45 apparent differentially expressed genes in intermediate B cells; none remained significant after restriction to mixed-age pools and within-pool correction. These panels are grouped because both diagnose inferential failure modes, rather than being treated as biological proof.

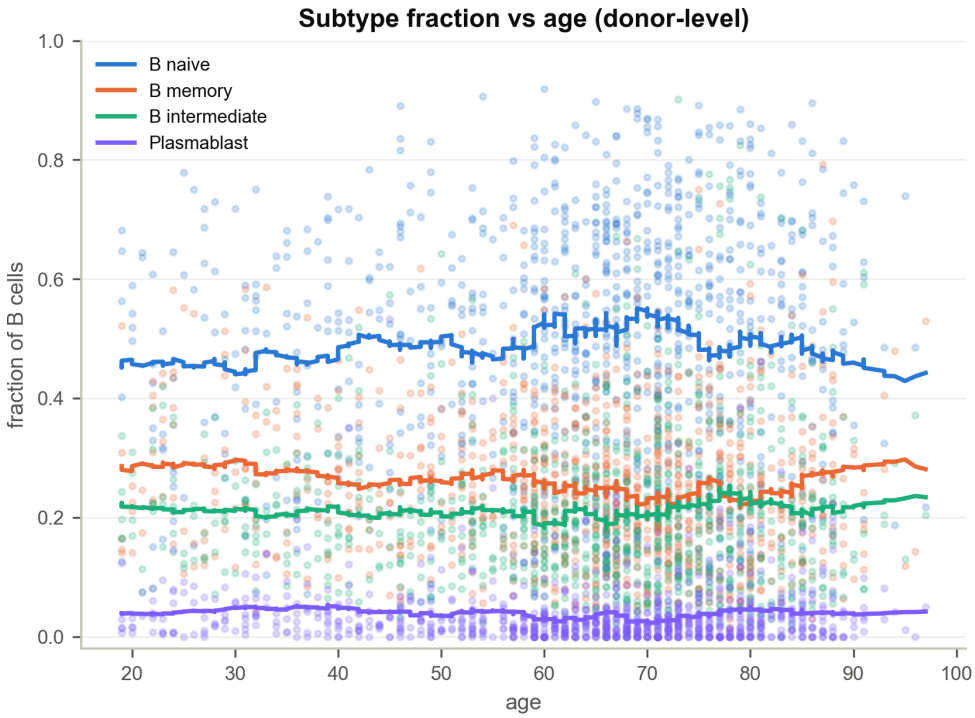

Figure 4: Major B-cell compartments remain largely stable. Donor-level fractions are shown across age for naive, memory, intermediate B cells, and plasmablasts. Although the discrete memory label decreased and the intermediate label increased, the supplied analyses showed that their combined compartment changed by only 1.6 percentage points and was not significant. No separate original merged-compartment panel was present in the supplied reports; the combined estimate is therefore reported in the text rather than reconstructed.

3.3 B-cell aging is accompanied by coordinated subtype-intrinsic transcriptional remodeling

Despite the relative stability of major compartments, age-associated transcriptional changes were detected within naive, memory, and intermediate B cells. In memory B cells, *CD69*, *NR4A2*, *BTG1*, and *LGALS1* increased with age (Fig. 5; Supplementary Fig. 10). Although the effect of any individual gene was modest, these genes collectively marked repeated or low-level receptor stimulation, immune regulation, anti-proliferative signaling, and stress adaptation. The corresponding donor-level trajectories were gradual rather than dominated by a single age threshold.

Hallmark analysis provided a pathway-level view of these small but coordinated effects. TNF-α/NF-κB, apoptosis, and p53-associated programs increased with age across major B-cell subtypes, whereas MYC target programs decreased (Fig. 6). Naive B cells showed prominent interferon-α and interferon-γ response enrichment. In memory B cells, increased inflammatory and activation-associated signals coexisted with reduced MYC/E2F-associated growth and cell-cycle preparation. Spline models fit the age relationships substantially better than simple linear models, with reported Akaike information criterion improvements of 269–529, indicating that a per-decade linear estimate is an average summary rather than a complete description of the trajectory.

These findings support a state characterized by heightened inflammatory vigilance but reduced readiness to enter sustained growth and clonal expansion. They do not imply that older B cells are uniformly hyperactive or globally dysfunctional; rather, they indicate a coordinated shift in the balance between signal reception, stress adaptation, and proliferative competence.

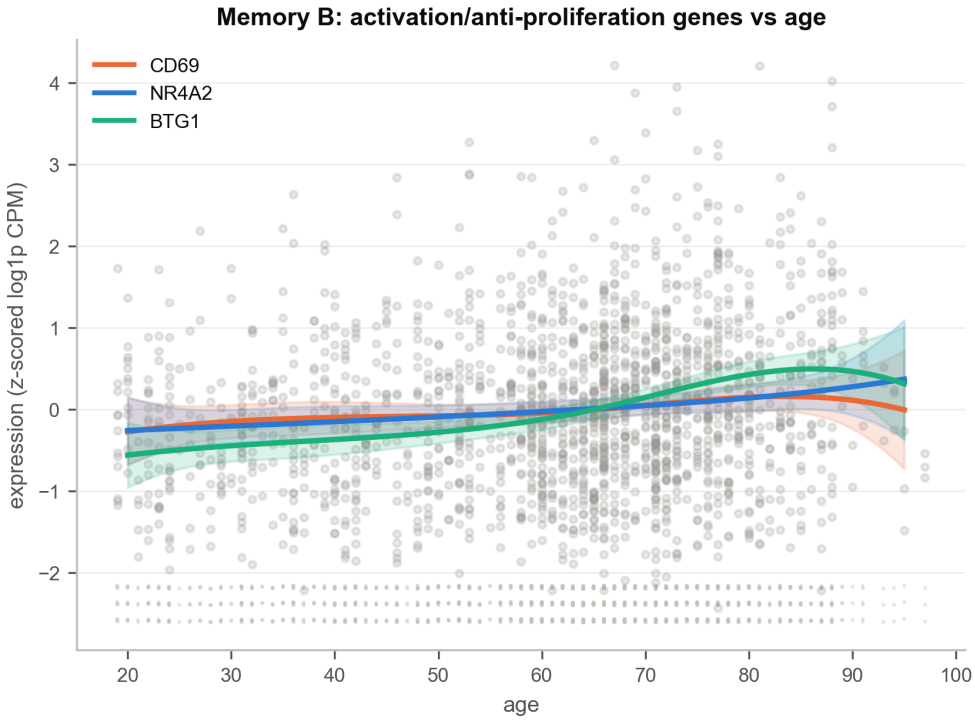

Figure 5: Age-associated expression trajectories within memory B cells. Donor-level trajectories are shown for representative activation, immune-regulatory, anti-proliferative, and stress-adaptation genes. The curves summarize gradual age dependence and should be interpreted together with the modest per-decade effect sizes and broad between-donor variability.

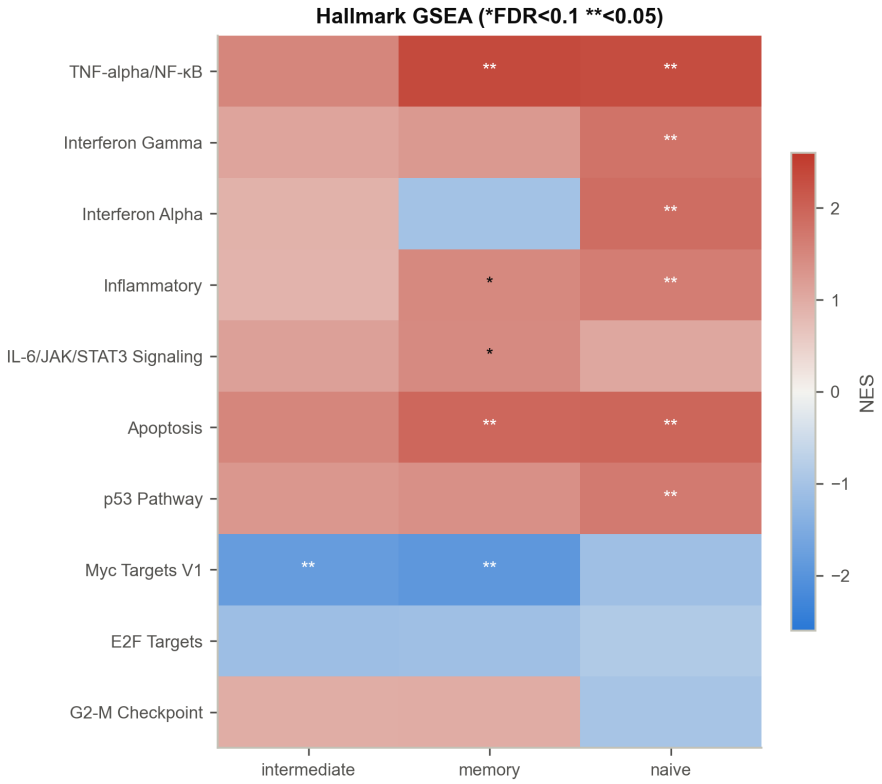

Figure 6: Aging remodels pathway activity within B-cell subtypes. Curated Hallmark normalized enrichment scores are displayed for intermediate, memory, and naive B cells. TNF-α/NF-κB, interferon, apoptosis, and p53-associated programs generally increased, whereas MYC-associated growth programs decreased. The long all-Hallmark young–old heatmaps are retained as sensitivity analyses in Supplementary Fig. 15.

3.4 FOXO3- and PAX5-associated programs define the most robust regulatory signals

Regulon analysis produced a clear evidence hierarchy after correction across the full transcription-factor testing space. FOXO3-associated target-gene programs increased with age in all three major B-cell subtypes (Fig. 7A; Supplementary Fig. 12). The estimated changes from age 40 to 80 years were $+0.143$ ULM units in naive B cells (0.34 donor standard deviations; FDR $= 0.0048$), $+0.173$ in memory B cells (0.44 standard deviations; FDR $= 0.0082$), and $+0.188$ in intermediate B cells (0.47 standard deviations; FDR $= 0.00489$). FOXO3 has established roles in cellular stress resistance, quiescence, metabolism, cell-cycle restraint, and apoptosis, and human *FOXO3* variation has been associated with longevity [Willcox et al., 2008]. The present result therefore identifies a shared FOXO3-associated adaptation program across three circulating B-cell subtypes, while not establishing direct FOXO3 activation or causality. The nonlinear memory-B-cell trajectory is shown separately in Supplementary Fig. 13.

A PAX5-associated identity-maintenance program decreased specifically in intermediate B cells. The estimated age-40-to-80 change was -0.250 ULM units (-0.67 donor standard deviations; FDR $= 1.12 \times 10^{-5}$). This result extends prior observations of low PAX5 in an age-associated B-cell population linked to poor influenza-vaccine response [Nipper et al., 2018] to a donor-level regulon signal in healthy intermediate B cells. It also offers a regulatory interpretation for the sensitivity of the memory–intermediate boundary, although direct chromatin or protein measurements will be required to establish whether PAX5 binding or abundance changes with age.

STAT1 in naive B cells and NF-κB-family programs in memory B cells showed agreement across regulon resources, inference methods, and matching Hallmark pathways. STAT1 activity correlated with interferon-γ enrichment ($r = 0.73$), and NF-κB-family scores correlated with TNF/NF-κB enrichment ($r = 0.68$–0.77). However, these signals did not pass the same full-space FDR threshold (STAT1 naive FDR approximately 0.105; NF-κB memory FDR approximately 0.504) and were therefore treated as convergent candidates rather than strict discoveries. The transcriptomic data could not reliably distinguish individual NF-κB-family members such as RELA, REL, and NFKB1.

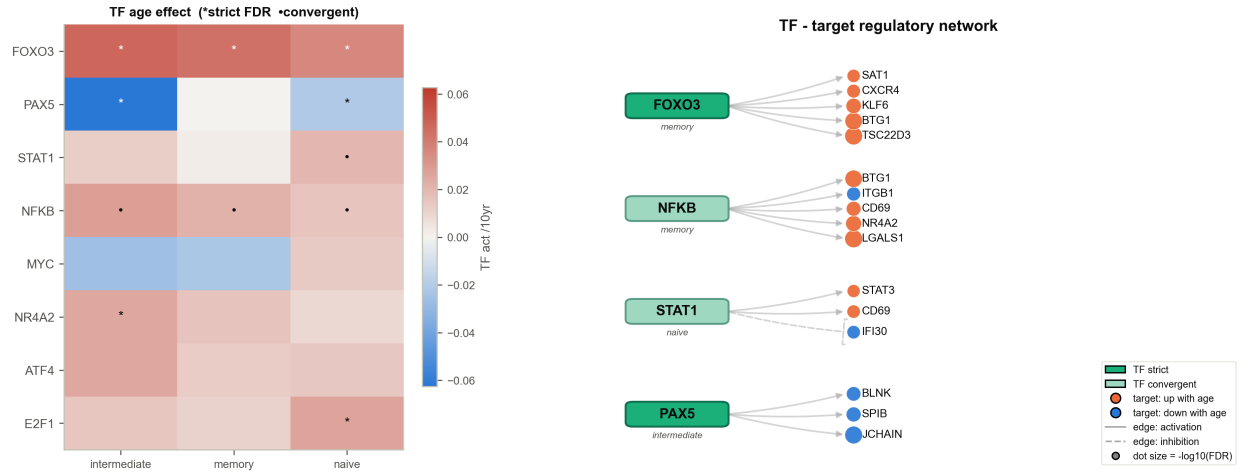

(A) TF-associated age-effect heatmap with evidence tiers.

(B) Simplified representative TF–target networks.

Figure 7: Shared FOXO3-associated adaptation and subtype-specific PAX5 decline. (A) FOXO3-associated programs increased across naive, memory, and intermediate B cells, whereas a PAX5-associated identity-maintenance program decreased in intermediate B cells. STAT1 and NF-κB are displayed as convergent candidates rather than strict full-space discoveries. **(B)** Representative target genes contributing to the inferred programs. Edges encode prior-knowledge relationships and do not demonstrate direct binding or causality in OneK1K donors.

Representative prior-knowledge networks summarize the genes contributing to the FOXO3, NF-κB, STAT1, and PAX5 scores (Fig. 7B), but do not establish binding, directionality, or causality in the OneK1K donors.

3.5 Core regulatory effects are directionally consistent across donor subsets

All six prespecified regulatory effects were directionally concordant between the discovery and replication halves (Fig. 8A). The FOXO3 estimates were similar in the two subsets for naive ($+0.14$ and $+0.17$), memory ($+0.16$ and $+0.20$), and intermediate ($+0.22$ and $+0.22$) B cells. The PAX5 estimate in intermediate B cells was likewise consistent (-0.23 and -0.29). STAT1 and NF-κB retained the same direction but had weaker replication estimates, consistent with their convergent rather than strict classification. Five of six age-by-sex interaction tests were not significant; the nominal FOXO3-by-sex interaction in intermediate B cells ($P = 0.043$) was exploratory and was not significant after accounting for the six tests. These results indicate that the principal effects are small but reproducible within independent donor subsets of the same cohort.

3.6 Young-versus-old contrasts expose batch sensitivity and analytical scale dependence

A dichotomous young-versus-old analysis provided an instructive challenge test. In the unadjusted model, intermediate B cells contained 45 significant genes, all higher in older donors and enriched for immunoglobulin and secretory-processing genes (Fig. 3B). The test-statistic inflation factor was 2.12. After restriction to pools containing both young and old donors and adjustment for pool, no subtype retained a significant differentially expressed gene. This 45-to-0 change demonstrates that apparently strong age-associated gene lists can arise from incomplete control of pool structure.

At the all-B level, within-pool Hallmark GSEA nevertheless identified strong metabolic signals in older donors, including oxidative phosphorylation, mTORC1 signaling, fatty-acid metabolism, glycolysis, unfolded-protein response, and E2F targets (Supplementary Fig. 15). The positive E2F signal differs from the reduced MYC/E2F preparedness observed in the primary subtype-resolved continuous-age analysis. Because the two analyses differ in aggregation level, age parameterization, gene filtering, and sample composition, the all-B young-versus-old result is treated as a sensitivity analysis rather than merged with the subtype-level model. This scale dependence reinforces the need to state precisely whether an aging signal reflects all B cells, a particular subtype, continuous age, or an extreme-group contrast.

The decade-level variance analysis did not support a general increase in transcriptomic variability with age. Across 9,401 globally expressed genes, mean variance showed little association with decade (Spearman $\rho = 0.167$, $P = 0.693$), both before and after pool residualization. Variance increased within the unadjusted age-associated gene set, but the decade-level trend was attenuated and no longer significant after pool residualization (ρ from 0.762, $P = 0.028$, to

0.286, $P = 0.493$). Thus, healthy B-cell aging was not characterized by a genome-wide loss of expression stability (Supplementary Fig. 18). Decade-level expression trajectories and the associated heatmap are shown in Supplementary Figs. 16 and 17.

3.7 An integrated model of B-cell aging

Together, the composition, expression, pathway, regulon, and replication analyses support a model in which healthy B-cell aging is dominated by coordinated state remodeling rather than wholesale depletion of the major B-cell compartments. Shared FOXO3-associated stress adaptation is superimposed on subtype-resolved changes in interferon vigilance, chronic NF-κB-associated stimulation, proliferative readiness, and PAX5-associated identity maintenance (Fig. 8B).

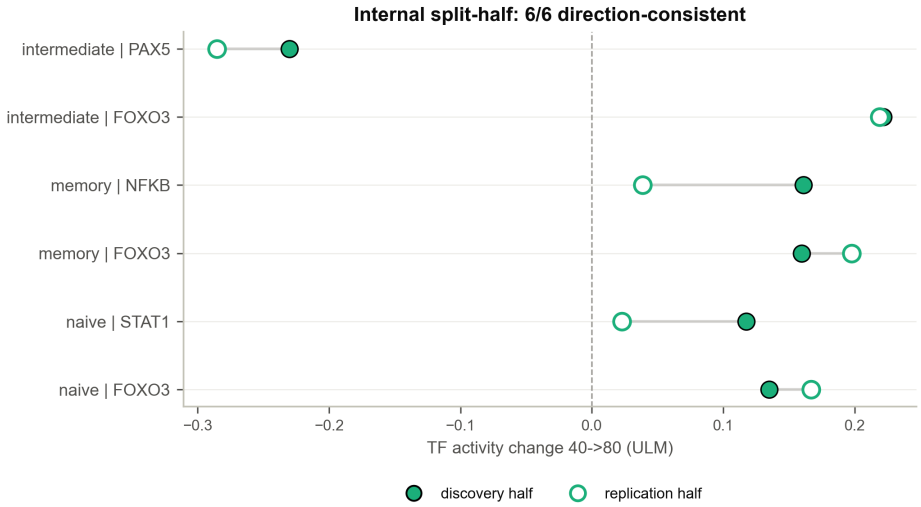

(A) Discovery and replication effects for six core programs.

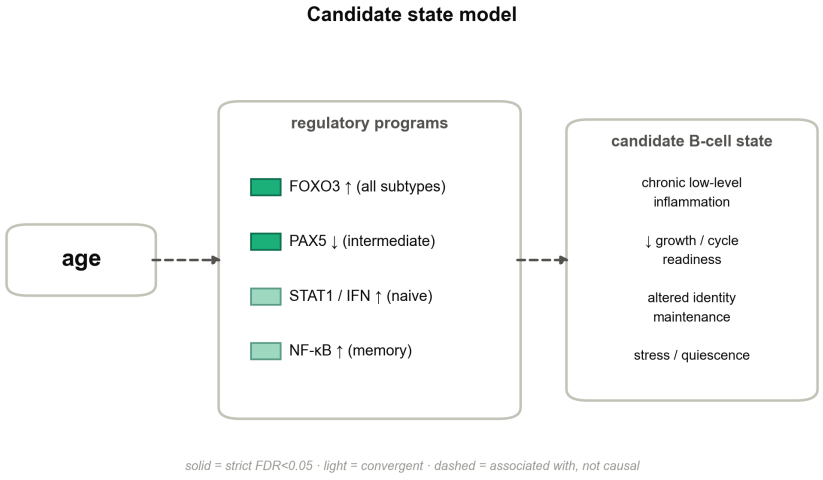

(B) Integrated candidate model of B-cell aging.

Figure 8: Core regulatory effects reproduce across donor subsets and converge on a candidate aging state. (A) All six prespecified effects were directionally concordant between discovery and replication donor subsets, with the strict FOXO3 and PAX5 effects showing the closest agreement in magnitude. **(B)** Age is associated with shared FOXO3-related stress adaptation, reduced PAX5-associated identity maintenance in intermediate B cells, and convergent STAT1/IFN and NF-κB programs. Dashed arrows denote association rather than causality.

4 Discussion

This population-scale analysis supports a model of healthy human B-cell aging in which regulatory-state remodeling is more prominent than major compartment loss. The central distinction is between discrete labels and the biological continuum that those labels approximate. Memory B-cell frequency declined and intermediate B-cell frequency increased when analyzed as separate clusters, yet the combined compartment was largely stable and a continuous memory–intermediate score did not shift with age. These results argue against describing the data as a simple depletion of memory B cells or as a global migration of cells along the memory–intermediate axis. A more accurate interpretation is that age is associated with modest redistribution near a cluster boundary, superimposed on broader within-subtype transcriptional changes.

The subtype-intrinsic changes converged on an apparently paradoxical state: stronger inflammatory and stress-associated signaling, but weaker proliferative readiness. In naive B cells, interferon-associated programs suggested heightened antiviral-like vigilance. In memory B cells, *CD69*, *NR4A2*, *BTG1*, and *LGALS1* increased together with TNF/NF-κB, apoptosis, and p53-associated pathways, whereas MYC/E2F-associated growth programs declined. This combination may help reconcile two recurring observations in immune aging: older immune cells can show evidence of chronic stimulation while mounting weaker expansion after a new antigenic challenge. The present transcriptomic data do not directly measure clonal expansion, but they provide a population-level molecular framework that can be tested in stimulation and vaccination studies.

The strongest regulatory finding was the shared increase in FOXO3-associated target programs across naive, memory, and intermediate B cells. FOXO3 is a plausible coordinator of stress resistance, quiescence, metabolic adaptation, cell-cycle control, and survival, and *FOXO3* genetic variation has repeatedly been associated with human longevity [Willcox et al., 2008]. Our result should be viewed as a previously underappreciated candidate axis rather than a claim of direct FOXO3 activation. Regulon scores are inferred from coordinated target-gene expression and can be influenced by overlapping regulatory networks. Protein localization, phosphorylation, chromatin occupancy, and perturbation experiments are required to establish mechanism.

The decrease in a PAX5-associated program in intermediate B cells provides a second, subtype-specific axis. PAX5 is required to maintain B-cell identity and function throughout B-cell development [Nutt et al., 1999, Cobaleda et al., 2007]. Nipper et al. [2018] previously linked low PAX5 expression in an age-associated B-cell population to reduced influenza-vaccine antibody responses. The present analysis does not replicate that clinical association, because vaccine response was not measured. Instead, it extends the observation to a large healthy cohort and localizes it to the regulon level in intermediate B cells. This may represent altered identity maintenance within a memory-adjacent state, but direct PAX5 protein and chromatin assays are needed.

The relationship to the study by Sopena-Rios et al. [2026] requires explicit delineation. Their analysis was immune-wide and centered on sex-specific trajectories, including female-predominant remodeling in T-cell and monocyte compartments and a male-restricted expansion of a CLL-precursor-like B-cell state. The present analysis instead asks whether conventional B-cell compartments are lost with age and whether donor-level subtype-intrinsic programs converge on shared or subtype-specific regulatory axes. The two studies are therefore complementary but statistically non-independent. Agreement on the importance of age, sex, continuous cellular state, and B-cell heterogeneity increases biological plausibility, but only validation in a separate cohort can establish external reproducibility.

STAT1 and NF-κB were supported by multiple lines of evidence but did not meet the global FDR threshold. This distinction is important. Interferon and NF-κB activation are well-established features of immune aging, so a candidate-restricted analysis could easily overstate their statistical strength. By correcting over the full transcription-factor space, we retained them as biologically coherent, convergent candidates while reserving the strict discovery tier for FOXO3 and PAX5. A similar discipline was necessary for the apparent 45-gene young-versus-old signature in intermediate B cells, which disappeared after within-pool correction.

The difference between the subtype-resolved continuous-age GSEA and the all-B extreme-age GSEA deserves explicit attention. The former indicated reduced MYC/E2F preparedness in memory-related subtypes, whereas the latter showed positive E2F and metabolic enrichment in old all-B samples. These findings are not directly interchangeable. Aggregating all B cells allows compositional and subtype-specific effects to mix, while dichotomizing age changes the estimand and gives disproportionate weight to the extremes of an uneven age distribution. We therefore regard the all-B result as a model- and scale-specific sensitivity signal. Future work should reproduce both analyses in an independent cohort and use formal interaction models to determine whether metabolic responses differ by subtype or age range.

Several limitations constrain interpretation. The study is cross-sectional and cannot establish within-person trajectories. The cohort is predominantly of European ancestry, contains more older than younger donors, and lacks detailed control for lifetime infection history, vaccination, medication, and lifestyle. Plasmablasts, proliferating B cells, and explicitly

defined age-associated B-cell populations were too sparse for definitive analysis. The main regulatory findings are computational inferences rather than measurements of protein activity or chromatin binding. NF-κB-family members could not be distinguished reliably. STAT1 and NF-κB did not pass the strict full-space FDR threshold. Finally, split-half consistency is not a substitute for external replication.

The highest-priority next steps are therefore focused validation rather than expansion of the candidate list. The FOXO3 and PAX5 regulon findings should be tested in independent, ancestrally diverse cohorts with comparable donor-level analysis. Protein-level assays should assess FOXO3 localization, PAX5 abundance and chromatin occupancy, STAT1 phosphorylation, and NF-κB nuclear translocation. Functional experiments should measure MYC induction, cell-cycle entry, clonal expansion, antibody secretion, and vaccine response after controlled B-cell stimulation. Longitudinal sampling would help distinguish stable age-associated differences from transient inflammatory or exposure-related states.

In conclusion, the data support a model in which the major B-cell compartments remain broadly present across the adult lifespan, while the cells within those compartments undergo small but coordinated regulatory changes. A shared FOXO3-associated stress-adaptation program, an intermediate-B-cell-specific reduction in PAX5-associated identity maintenance, stronger interferon and NF-κB-related vigilance, and weaker MYC/E2F-related proliferative readiness together define an inflammation-alert and stress-adapted state that may be less prepared for clonal expansion. This framework reframes B-cell aging as regulatory-state remodeling rather than simple cell loss.

Data availability

The source OneK1K dataset is available under the access and citation terms described by Yazar et al. [2022] and the OneK1K project. The processed donor-by-subtype pseudobulk matrices, analysis scripts, parameter files, and figure-source data should be deposited in [TO CONFIRM: repository and accession] before publication, subject to the original data-use agreement.

Code availability

Analysis code should be released at [TO CONFIRM: GitHub/Zenodo link], including environment files, software versions, random seeds for the split-half assignment, gene-set versions, regulon-resource versions, and scripts used to generate every main and supplementary figure.

Ethics statement

[TO CONFIRM: Insert the ethics approval, informed-consent statement, and secondary-use authorization exactly as specified in the OneK1K documentation and the authors' institutional requirements.]

Acknowledgments

We thank the OneK1K investigators and study participants for generating and sharing the single-cell dataset. [TO CONFIRM: Insert funding, institutional support, and individual acknowledgments.]

Author contributions

Conceptualization: [ ]; Methodology: [ ]; Software: [ ]; Formal analysis: [ ]; Investigation: [ ]; Data curation: [ ]; Visualization: [ ]; Writing–original draft: [ ]; Writing–review and editing: [ ]; Supervision: [ ]; Funding acquisition: [ ].

Competing interests

The authors declare [TO CONFIRM: no competing interests / insert disclosures].

Submission checklist

The following fields must be verified before submission:

- final author list, affiliations, corresponding-author details, funding, and contributions;
- OneK1K ethics and informed-consent wording, data accession, and the reason 981 rather than 982 donors were retained;
- B-cell re-annotation workflow, marker genes, clustering parameters, and donor–subtype minimum-cell thresholds;
- the primary continuous-age expression model, normalization, filtering, covariates, spline degrees of freedom, and software versions;
- construction of the memory–intermediate continuous score and all FDR correction families;
- verification of every numerical value and figure against final source data; and
- a public code and processed-data repository, or a clear data-access statement.

A Supplementary figures

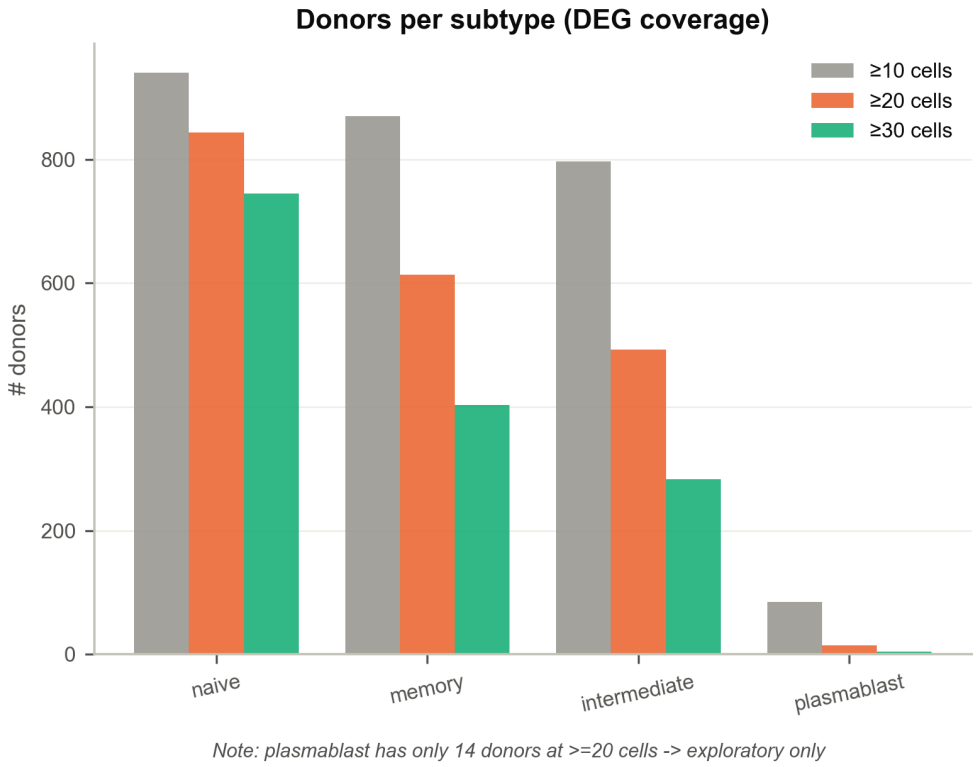

Figure 9: Supplementary Figure S1. Donor coverage across B-cell subtypes. Numbers of donors meeting alternative minimum cell-count thresholds. Plasmablast analyses were exploratory because few donors met higher thresholds.

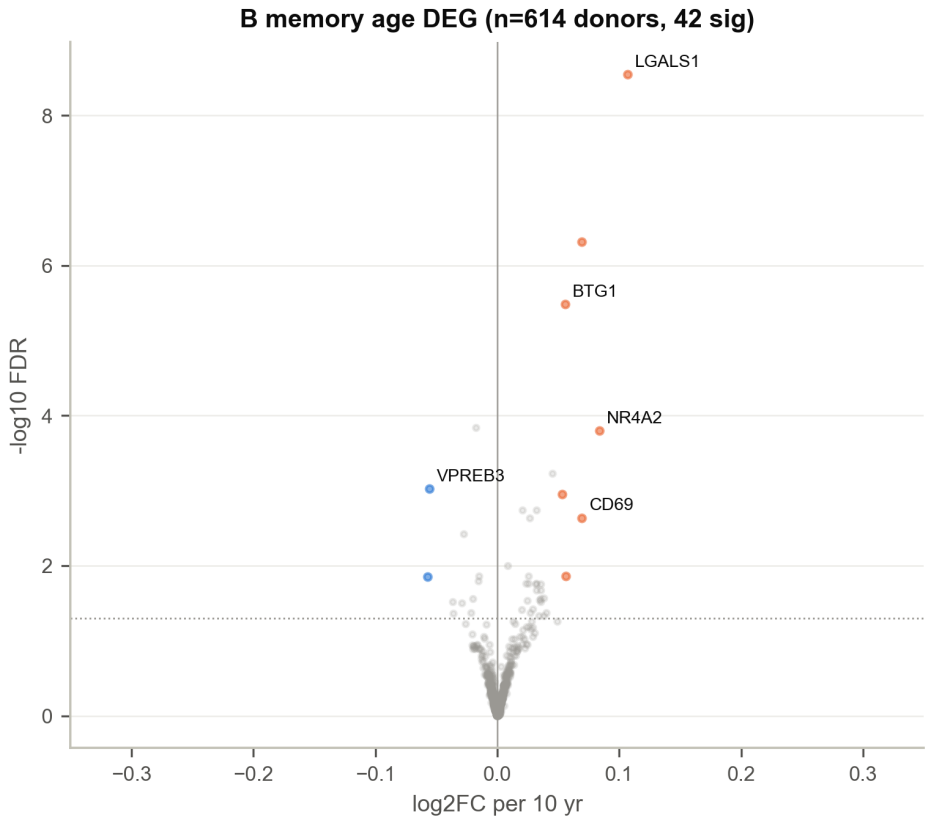

Figure 10: Supplementary Figure S2. Memory-B-cell continuous-age differential-expression summary. Most effects were small; representative age-associated genes include *LGALS1*, *BTG1*, *NR4A2*, and *CD69*.

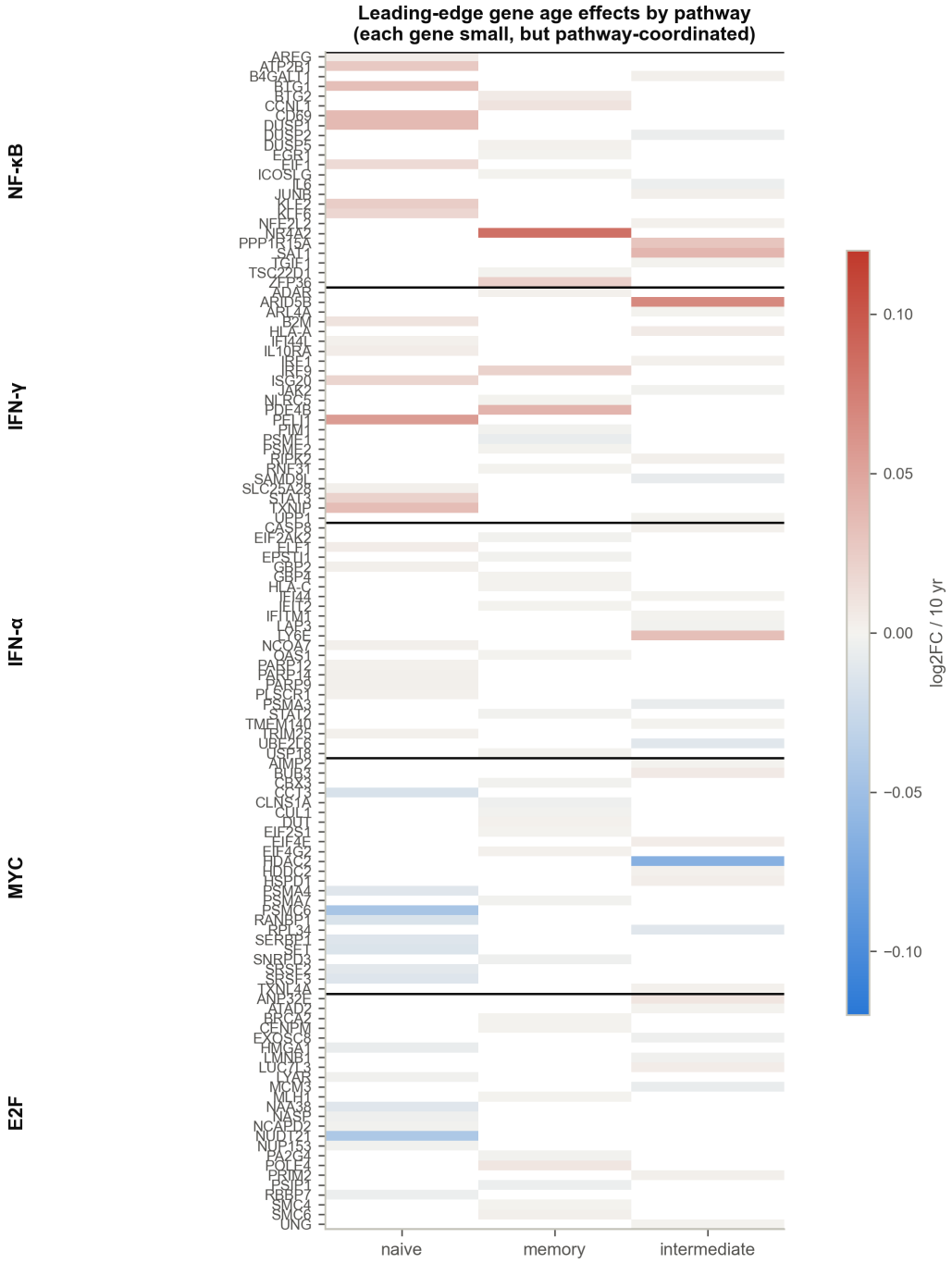

Figure 11: Supplementary Figure S3. Leading-edge gene effects underlying selected pathways. Individual gene effects are small, but groups of pathway genes shift coherently across subtypes.

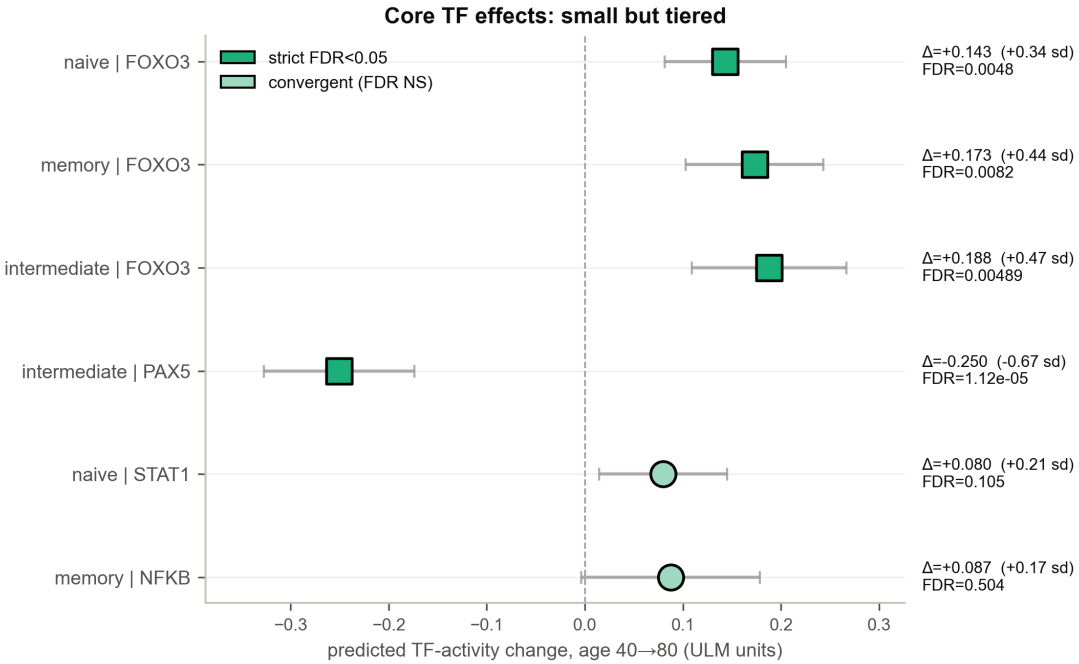

Figure 12: Supplementary Figure S4. Magnitudes of the six core inferred regulatory effects. Predicted age-40-to-80 changes are shown with confidence intervals, donor-standard-deviation scaling, false-discovery rates, and strict or convergent evidence tiers.

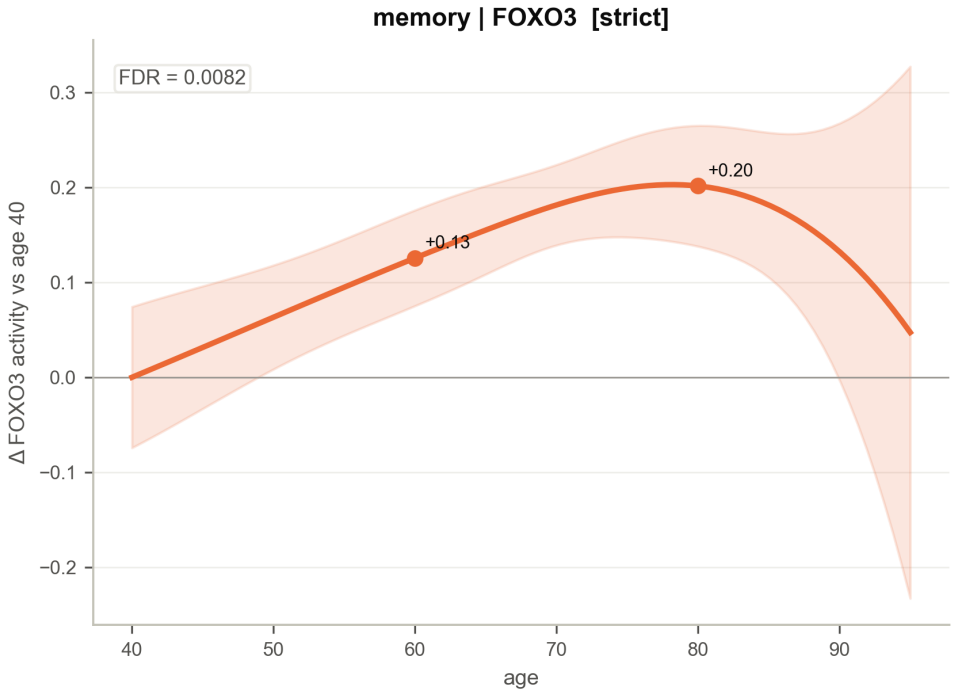

Figure 13: Supplementary Figure S5. Nonlinear age trajectory of the memory-B-cell FOXO3-associated program. The line is expressed relative to the age-40 baseline; wide uncertainty at the oldest ages reflects limited observations at the distributional edge.

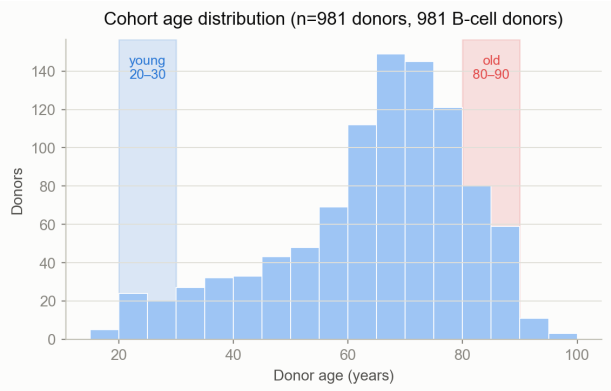

(A) Age distribution and extreme-age bands.

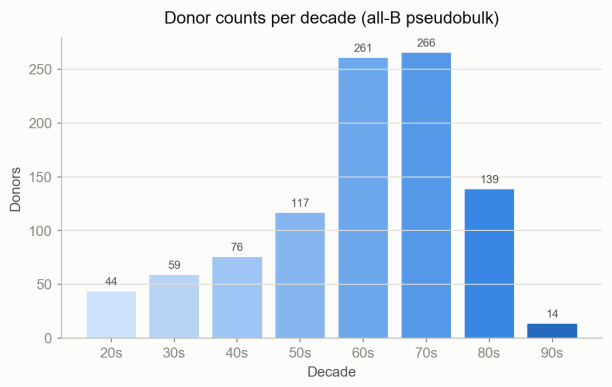

(B) Donor counts by decade.

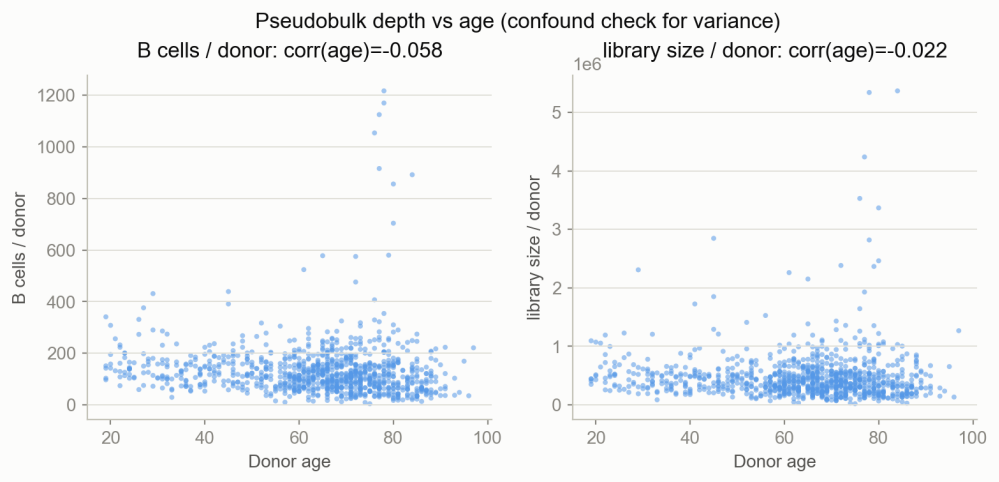

(C) B-cell number and library size versus age.

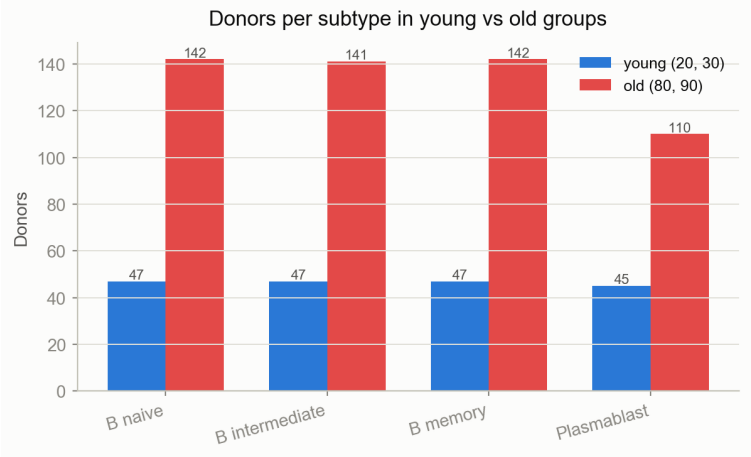

(D) Subtype donor coverage in young and old groups.

Figure 14: Supplementary Figure S6. Cohort and depth checks for the extreme-age sensitivity analysis. The panels reproduce the QC organization of the young-versus-old report rather than combining these checks with biological result panels.

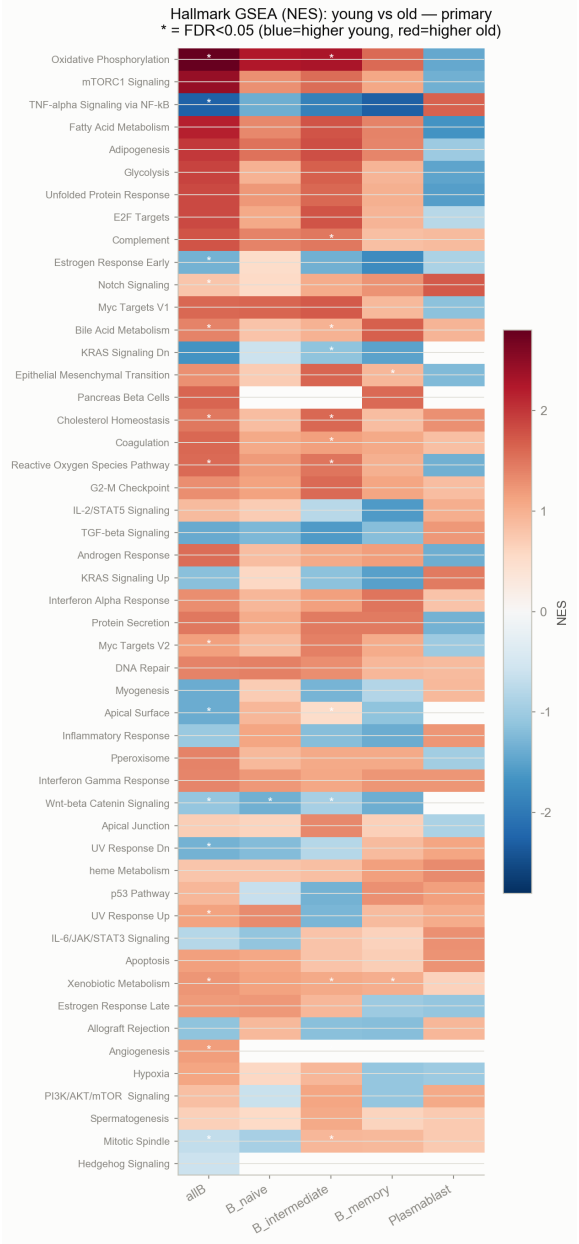

(A) Primary young–old model.

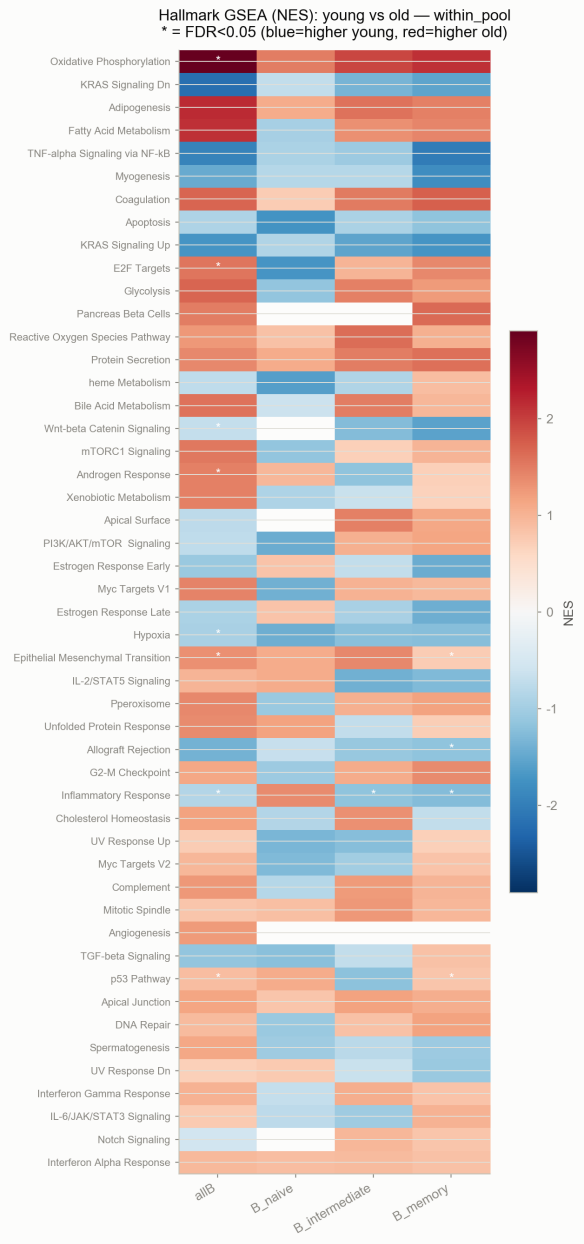

(B) Within-pool sensitivity model.

Figure 15: Supplementary Figure S7. Full Hallmark GSEA for the all-B extreme-age analysis. These heatmaps are retained as a separate sensitivity analysis and are not merged with the subtype-resolved continuous-age heatmap in Fig. 6.

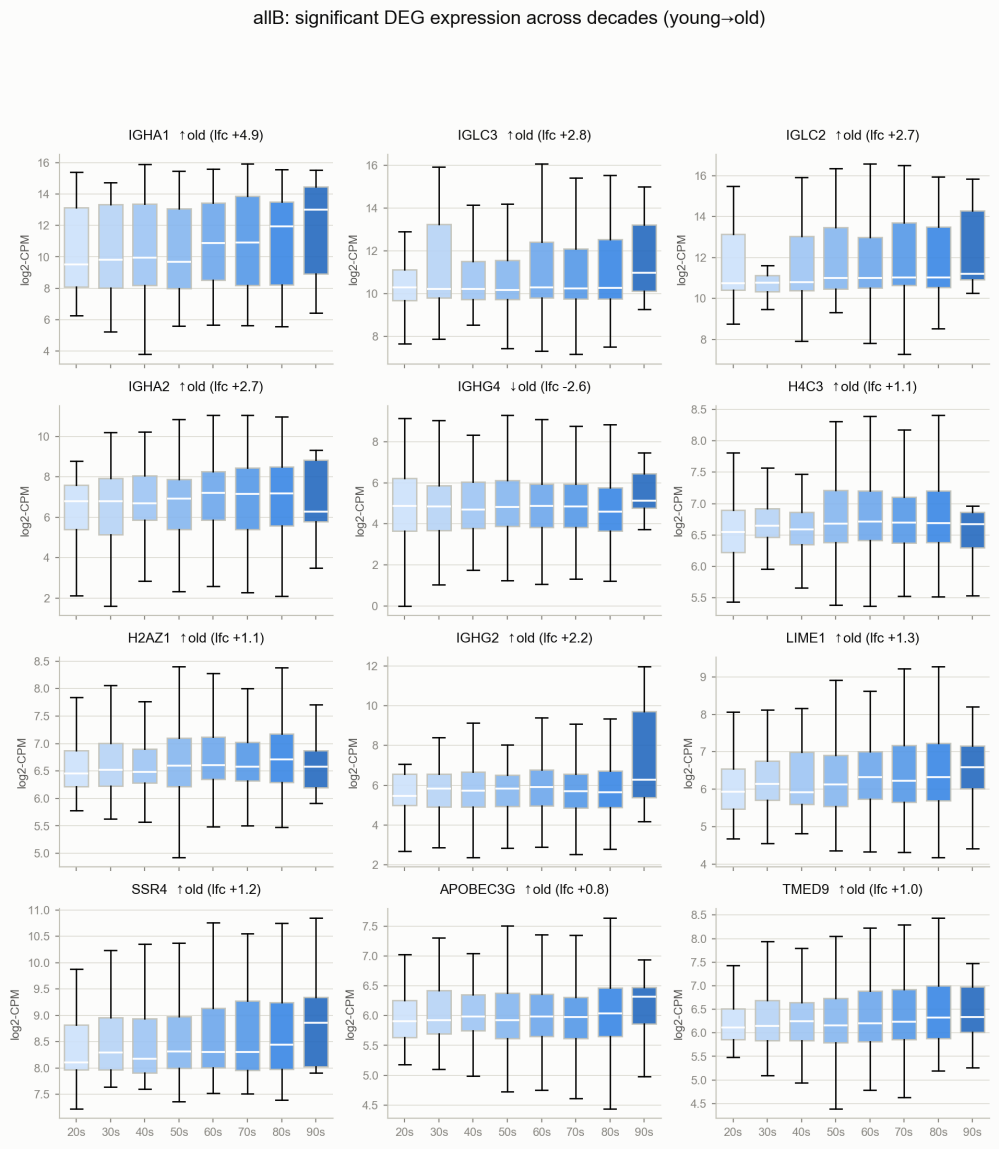

(A) Decade-level boxplots for representative genes.

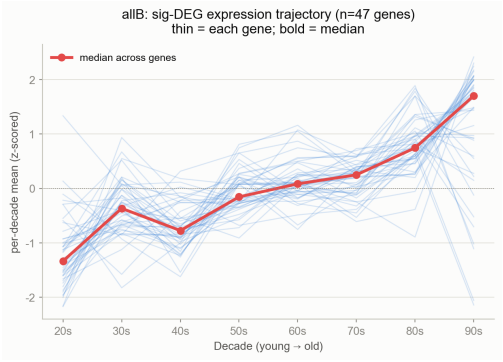

(B) Standardized trajectories across decades.

Figure 16: Supplementary Figure S8. Decade-level expression trajectories in the extreme-age gene set. The boxplots and standardized trajectory summarize the same decade-binned analysis and are kept separate from the continuous-age subtype results in the main figures.

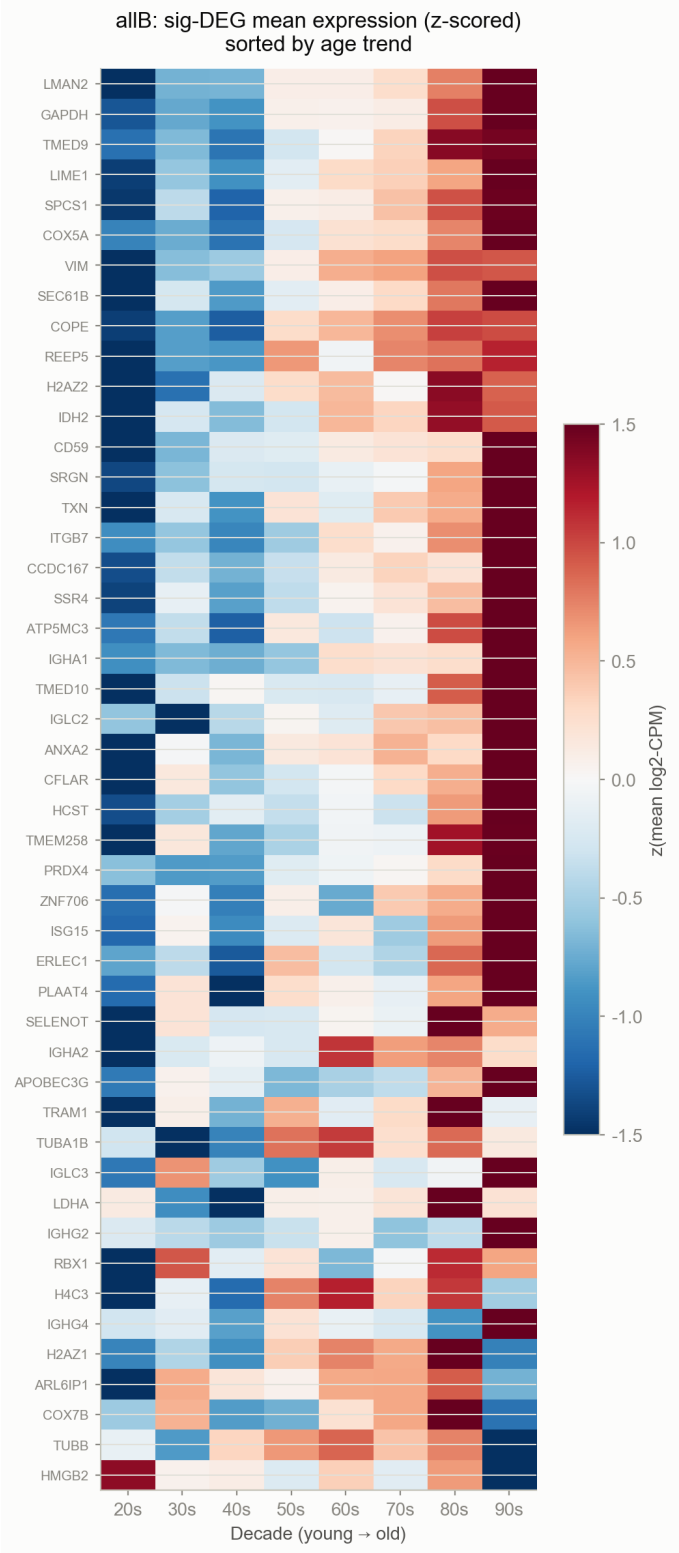

Figure 17: Supplementary Figure S9. Decade-level expression heatmap. Standardized mean expression of the reported extreme-age gene set across decade bins, ordered by age trend.

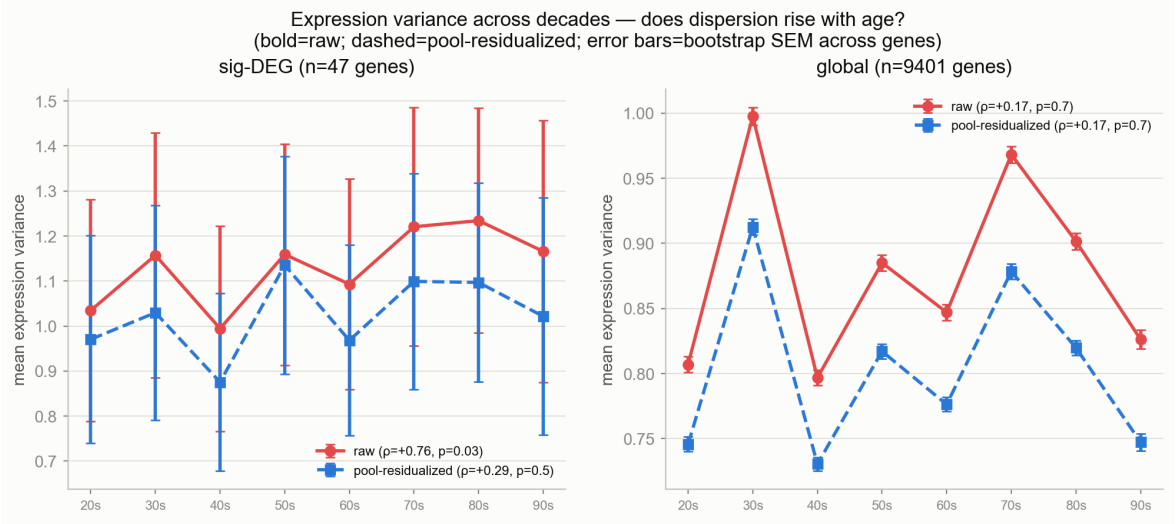

Figure 18: Supplementary Figure S10. Expression variance across decades. Global expression variance did not increase systematically with age. The apparent trend in the unadjusted differential-gene set was attenuated after pool residualization.

References

K. Goodwin, C. Viboud, and L. Simonsen. Antibody response to influenza vaccination in the elderly: a quantitative review. *Vaccine*, 24(8):1159–1169, 2006. doi: 10.1016/j.vaccine.2005.08.105.

Daniela Frasca, Ana Maria Landin, Susan C. Lechner, J. G. Ryan, Robert Schwartz, Richard L. Riley, and Bonnie B. Blomberg. Aging down-regulates the transcription factor e2a, activation-induced cytidine deaminase, and ig class switch in human b cells. *Journal of Immunology*, 180(8):5283–5290, 2008. doi: 10.4049/jimmunol.180.8.5283.

Denis A. Mogilenko, Irina Shchukina, and Maxim N. Artyomov. Immune ageing at single-cell resolution. *Nature Reviews Immunology*, 22:484–498, 2022. doi: 10.1038/s41577-021-00646-4.

Maria Terekhova, Alex Swain, Pavla Bohacova, et al. Single-cell atlas of healthy human blood unveils age-related loss of nkg2c+gzmb- cd8+ memory t cells and accumulation of type 2 memory t cells. *Immunity*, 56:2836–2854, 2023.

Y. Hao, P. O'Neill, M. S. Naradikian, J. L. Scholz, and M. P. Cancro. A b-cell subset uniquely responsive to innate stimuli accumulates in aged mice. *Blood*, 118(5):1294–1304, 2011. doi: 10.1182/blood-2011-01-330530.

Anatolij V. Rubtsov, Kira Rubtsova, Alexander Fischer, Rita T. Meehan, Jason Z. Gillis, John W. Kappler, and Philippa Marrack. Toll-like receptor 7-driven accumulation of a novel cd11c-positive b-cell population is important for the development of autoimmunity. *Blood*, 118(5):1305–1315, 2011. doi: 10.1182/blood-2011-01-331462.

A. J. Nipper, M. J. Smithey, R. C. Shah, D. H. Canaday, and A. L. Landay. Diminished antibody response to influenza vaccination is characterized by expansion of an age-associated b-cell population with low pax5. *Clinical Immunology*, 193:80–87, 2018. doi: 10.1016/j.clim.2018.02.003.

Stephen L. Nutt, Brendan Heavey, Antonius G. Rolink, and Meinrad Busslinger. Commitment to the b-lymphoid lineage depends on the transcription factor pax5. *Nature*, 401:556–562, 1999. doi: 10.1038/44076.

Carmen Cobaleda, Andrea Schebesta, Alessandro Delogu, and Meinrad Busslinger. Pax5: the guardian of b cell identity and function. *Nature Immunology*, 8(5):463–470, 2007. doi: 10.1038/ni1454.

Seyhan Yazar, Jose Alquicira-Hernandez, Kristof Wing, Anne Senabouth, M. Grace Gordon, Stacey Andersen, Qinyi Lu, Antonia Rowson, Thomas R. P. Taylor, Linda Clarke, Katia Maccora, Christine Chen, Anthony L. Cook, Chun Jimmie Ye, Kirsten A. Fairfax, Alex W. Hewitt, and Joseph E. Powell. Single-cell eqtl mapping identifies cell type-specific genetic control of autoimmune disease. *Science*, 376(6589):eabf3041, 2022. doi: 10.1126/science.abf3041.

Maria Sopena-Rios, Aida Ripoll-Cladellas, Fatemeh Omidi, Sara Ballouz, Jose Alquicira-Hernandez, Roy Oelen, Alex W. Hewitt, Lude Franke, Monique G. P. van der Wijst, Joseph E. Powell, and Marta Mele. Single-cell analysis of the human immune system reveals sex-specific dynamics of immunosenescence. *Nature Aging*, 6:932–949, 2026. doi: 10.1038/s43587-026-01099-x.

Jordan W. Squair, Matthieu Gautier, Claudia Kathe, et al. Confronting false discoveries in single-cell differential expression. *Nature Communications*, 12:5692, 2021. doi: 10.1038/s41467-021-25960-2.

Helena L. Crowell, Charlotte Soneson, Pierre-Luc Germain, et al. muscat detects subpopulation-specific state transitions from multi-sample multi-condition single-cell transcriptomics data. *Nature Communications*, 11:6077, 2020. doi: 10.1038/s41467-020-19894-4.

Aravind Subramanian, Pablo Tamayo, Vamsi K. Mootha, et al. Gene set enrichment analysis: a knowledge-based approach for interpreting genome-wide expression profiles. *Proceedings of the National Academy of Sciences of the United States of America*, 102(43):15545–15550, 2005. doi: 10.1073/pnas.0506580102.

Arthur Liberzon, Chet Birger, Helga Thorvaldsdottir, Mahmoud Ghandi, Jill P. Mesirov, and Pablo Tamayo. The molecular signatures database hallmark gene set collection. *Cell Systems*, 1(6):417–425, 2015. doi: 10.1016/j.cels.2015.12.004.

Pau Badia-i Mompel, Jesus Velez Santiago, Jana Braunger, et al. decoupler: ensemble of computational methods to infer biological activities from omics data. *Bioinformatics Advances*, 2(1):vbac016, 2022. doi: 10.1093/bioadv/vbac016.

Luz Garcia-Alonso, Christian H. Holland, Mahmoud M. Ibrahim, Denes Turei, and Julio Saez-Rodriguez. Benchmark and integration of resources for the estimation of human transcription factor activities. *Genome Research*, 29(8):1363–1375, 2019. doi: 10.1101/gr.240663.118.

Sophia Muller-Dott, Eirini Tsirvouli, Miguel Vazquez, et al. Expanding the coverage of regulons from high-confidence prior knowledge for accurate estimation of transcription factor activities. *Nucleic Acids Research*, 51(20):10934–10949, 2023. doi: 10.1093/nar/gkad841.

Bradley J. Willcox, Timothy A. Donlon, Qimei He, et al. Foxo3a genotype is strongly associated with human longevity. *Proceedings of the National Academy of Sciences of the United States of America*, 105(37):13987–13992, 2008. doi: 10.1073/pnas.0801030105.